Macromolecules

pubs.acs.org/Macromolecules

Article

Isotropic-to-Nematic Transition in Salt-Free Polyelectrolyte Coacervates from Coarse-Grained Simulations

Boyuan Yu, Heyi Liang, Artem M. Rumyantsev, and Juan J. de Pablo*

Cite This: https://doi.org/10.1021/acs.macromol.2c01674

Read Online

ACCESS | Metrics & More | Article Recommendations | Supporting Information

ABSTRACT: Recent interest in complex coacervation between oppositely charged polyelectrolytes (PEs) has been fueled by its relevance to biology in the context of membraneless organelle formation within living cells. For PEs with limited flexibility (such as double-stranded DNA), theoretical treatments and recent experiments have reported the emergence of liquid crystalline order (LCO) within the resulting coacervate phases. In this work, we study the underlying physics of this phenomenon using coarse-grained molecular dynamics simulations of symmetric semiflexible−semiflexible and asymmetric semiflexible−flexible coacervates. By comparing coacervates with the corresponding semidilute solutions of neutral polymers, we demonstrate that the presence of Coulomb interactions in coacervates facilitates orientational ordering, in agreement with theoretical predictions. Quantitative comparisons between our simulations and theory indicate that, for asymmetric nematic coacervates, the strong orientational ordering of stiff polyanions induces a weak ordering of the flexible polycations—an effect that was not anticipated by available theoretical studies. Simulations reveal that, for nematic coacervates, the preferred orientation of the PE chains at the liquid−liquid coacervate−supernatant interface is parallel, and the alignment of semiflexible PEs is homogeneous. The results presented here provide new molecular-level insights into the intra-coacervate LCO and will help motivate further experimental and theoretical activities in this area.

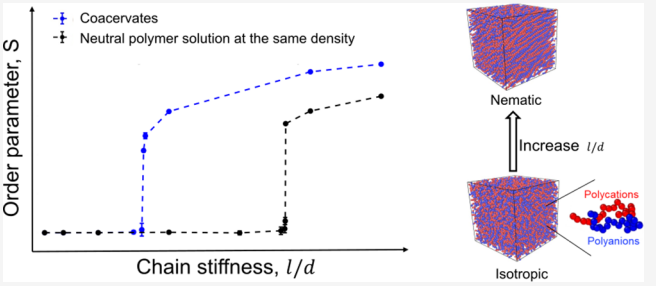

1. INTRODUCTION

Mixtures of oppositely charged polyelectrolytes (PEs) in solution can undergo phase separation into a polymer-rich coacervate phase and a polymer-lean supernatant phase. This phenomenon is partly responsible for the liquid−liquid phase separation (LLPS) of biological macromolecules,[1−3] which is important for intracellular organization[4−6] and the formation of membrane-less organelles[7−10] within living cells. Recent studies have also shown that complex coacervation between charged biopolymers, such as polypeptides and polynucleotides, can be a potential route of prebiotic evolution because the coacervate droplets provide molecular crowding and compartmentalized environments, which are necessary to achieve high efficiency of the underlying biochemical reactions.[6,11−13]

Extensive studies have sought to understand how the equilibrium and rheological properties of complex coacervates can be altered by charge fraction, monomer sequence, added salt concentration, and so forth.[14−30] However, the majority of past work has focused on isotropic (and homogeneous rather than microphase separated[31−34]) coacervate phases. When considering coacervation in the context of bioPEs, an important feature is that polyanions, particularly double-stranded DNA (dsDNA) and/or polycations, have limited flexibility. It is known that semidilute solutions of neutral semiflexible polymers can exhibit liquid crystalline order (LCO) even at low polymer concentrations.[35−37] Phase transitions from disordered (isotropic) to ordered (nematic or smectic) states can be triggered by increasing the polymer concentration and chain stiffness.[35,38−41] It is therefore natural to expect that the orientational order could emerge in coacervates containing semiflexible PEs because the internal structure of coacervates is similar to that of semidilute solutions of neutral polymers.[26,42]

Experimental evidence of LCO was first reported by Shakya and King,[43] who studied coacervates formed from poly-L-lysine (PLL) and either single-stranded DNA (ssDNA) or dsDNA. It was shown that the secondary phase transition from isotropic to a LC cholesteric state takes place within coacervate droplets when they contain stiff dsDNA but is absent if stiff DNA duplexes are replaced by flexible ssDNA.

Recently, Jia and Fraccia[11] considered PLL−dsDNA coacervates and reported a phase diagram expressed in terms of salt and polymer concentrations. This diagram included

Received: August 10, 2022
Revised: September 16, 2022

regions where an isotropic coacervate is found and other regions with several LC mesophases. The addition of salt was shown to trigger transitions from more ordered states to less ordered LC phases, namely, from a highly ordered columnar phase C_s to a uniaxial columnar phase C_U to a twisted nematic (cholesteric) phase N^*. Additional increases in the salt concentration resulted in a transition to the isotropic coacervate phase and, eventually, in the coacervate's dissolution.[11]

LCO of dsDNA was also observed in the cores of PE complex micelles composed of dsDNA and PLL-*b*-poly(ethylene glycol).[44] In this case, cryo-transmission electron microscopy studies revealed that stiff dsDNA rods are organized in the (uniaxial) columnar phase within the cylindrical micellar cores. Substituting stiff dsDNA with flexible ssDNA resulted in the breakdown of orientational order and in a change of the micellar morphology from worm-like to spherical.

The examples above serve to illustrate that liquid crystallinity in coacervates leads to a rich phase behavior; it is also believed to play an essential role in prebiotic molecular evolution. The higher polymer concentrations encountered in LC coacervates (as compared to their isotropic counterparts) promote selective uptake of biomolecules, and the orientational order facilitates more rapid and efficient polymerization of nucleic acids (non-enzymatic ligation) and peptides.[11,45−47]

Theoretical approaches based on the random phase approximation (RPA) have been developed to describe the phase behavior of symmetric coacervates formed from the oppositely charged rod-like PEs,[48] and that of asymmetric coacervates containing semiflexible polyanions and flexible polycations.[49] In both cases, isotropic-to-nematic (I−N) phase transitions at increasing coacervate densities have been predicted, and electrostatic interactions have been shown to facilitate the emergence of LCO.[48,49] While these past studies provide useful insights into the underlying physics of liquid crystallinity in systems that exhibit long-range Coulomb interactions, they have been limited to weakly charged, infinitely long, or perfectly stiff, rod-like PEs.[48,49] Molecular simulations provide a useful tool to bridge theoretical and experimental studies, and they can offer additional molecular-level insights into these systems. Additionally, they provide a means to directly corroborate some of the basic theoretical predictions of refs 48 and 49.

To the best of our knowledge, comprehensive simulation studies that address specifically intra-coacervate I−N transitions have not been reported before. The most relevant work on this topic is that of ref 50, where coarse-grained molecular dynamics (MD) were used to consider the complexation of long flexible polycations with short semiflexible polyanions. That study was focused on the role of chain flexibility on the density of the isotropic coacervate and the salt partitioning between the polymer-rich phase and the supernatant. The formation of nematic coacervates was not considered. Our work therefore represents a first attempt to provide a molecular-level understanding of orientational order in PE complex coacervates.

A unique feature of LC coacervates is that they represent a special type of LC, which is sensitive not only to the temperature and polymer concentration but also to the salt concentration. The addition of salt screens the orientation-dependent Coulomb interactions between the polyions and induces a nematic-to-isotropic (N−I) transition, even for a constant mesogen (i.e., polyions) concentration. The sensitivity of LC coacervates to this new stimulus could provide opportunities for the design of systems that are responsive to multiple orthogonal stimuli.

In the absence of salt, Coulomb interactions also alter the traditional behaviors observed in polymer liquid crystals. For example, neutral stiff polymers in an athermal solvent only undergo lyotropic phase transitions (Onsager model). In contrast, in PE systems, the presence of Coulomb interactions makes them sensitive to temperature, that is, the LC becomes thermotropic.

In the present study, we consider simple but representative salt-free coacervates and focus on the transition from the isotropic to the nematic state. We perform coarse-grained MD simulations of (1) symmetric semiflexible−semiflexible coacervates and (2) asymmetric semiflexible−flexible coacervates, both in an implicit solvent. The first, symmetric case was theoretically considered in ref 48; that work, however, dealt with only perfectly rod-like polymers but not semiflexible chains. The asymmetric system was studied theoretically in ref 49 and can be viewed as a minimal model for coacervates formed from dsDNA and PLL[43] or for other dsDNA-containing coacervate phases.

We aim to consider how increasing the stiffness of semiflexible chains in both systems induces the I−N transition and examine whether the predictions provided by the RPA-based theories are valid in systems with strongly charged short PEs. In particular, we elucidate the role of Coulomb and excluded volume interactions in the LCO by comparing coacervates to their corresponding neutral systems.

The interfacial properties of complex coacervates are also of great interest, as they play an important role in determining the functionality of polymeric materials.[51−56] Because the nematic phase is less symmetric than the isotropic and there is a preferential direction along which semiflexible PEs are aligned, the question of the relative orientation of the director and the coacervate interface (which is irrelevant for isotropic phases) arises naturally. For this reason, we also examine in some detail the preferential orientation of PE chains at the interface between the nematic coacervate and the supernatant.

Our paper is organized as follows. The details of our coarse-grained MD simulations are specified in Section 2. Section 3 presents our main results and consists of three parts. First, symmetric coacervates formed from semiflexible PEs of equal stiffness are considered in Subsection 3.1, where we demonstrate the formation of nematic coacervates and discuss the effect of electrostatic interactions on the I−N transition by comparing coacervates with the corresponding solutions of neutral polymers. Second, Subsection 3.2 is devoted to the study of asymmetric flexible−semiflexible coacervates. In Subsection 3.3, we discuss the orientation of semiflexible PEs at the coacervate−supernatant interface. Our findings are summarized in Section 4.

2. SIMULATION METHODS

The classic Kremer−Grest model[57] is used to represent PEs in an implicit solvent. Specifically, PE chains are modeled by spherical interaction sites (beads) connected by springs. The solvent is included implicitly for computational efficiency. As a result, solvent quality is controlled by the non-bonded interactions between the monomers. In our simulations, we consider good (athermal) solvent conditions for the polymer chains. The coacervate is electroneutral, and consists of an equal number of polyanions and polycations, both with chain length $N = 20$. Polyanions are fully charged semiflexible

https://doi.org/10.1021/acs.macromol.2c01674
Macromolecules XXXX, XXX, XXX−XXX

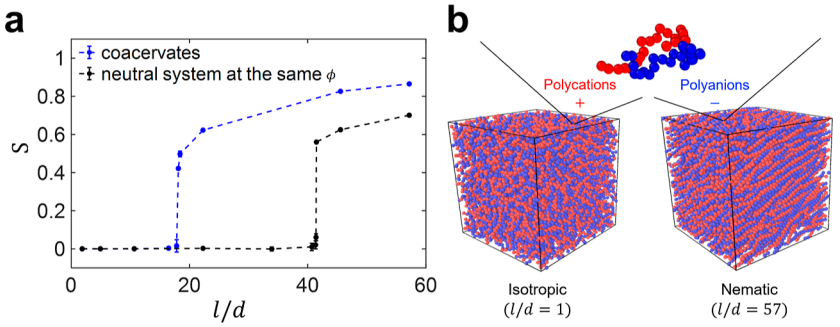

Figure 1. (a) Dependence of the order parameter S on the chain stiffness l/d for salt-free coacervates (blue curve) and the corresponding neutral semidilute solution of polymers at the same volume fraction ϕ (black curve) and (b) visualization of the salt-free coacervate in the isotropic and nematic states, $l/d = 1$ and $l/d = 57$, respectively. Polyanions and polycations are shown in blue and red. Simulation parameters are equal to $f_+ = f_- = 1.0$, $l_B/\sigma = 3$, and $N_+ = N_- = 20$.

chains while polycations can be either semiflexible or flexible chains, with a fraction of ionic beads $f_+ = 0.5$, 0.55, 0.6, 0.75, and 1.0. The total number of beads in the system is up to 31,000.

The connectivity of beads is provided by a finitely extensible nonlinear elastic (FENE) potential between adjacent neighbors along the polymer backbone

$$U_{\mathrm{FENE}} = -0.5KR_0^2 \ln\left[1 - \left(\frac{r}{R_0}\right)^2\right] \tag{1}$$

with $K = 30k_BT/\sigma^2$ and $R_0/\sigma = 1.5$.[57] All beads interact through a shifted and truncated Lennard–Jones (LJ) potential, which mimics good solvent conditions

$$U_{\mathrm{LJ}} = \begin{cases} 4\varepsilon\left[\left(\frac{\sigma}{r}\right)^{12} - \left(\frac{\sigma}{r}\right)^{6} - \left(\frac{\sigma}{r_c}\right)^{12} + \left(\frac{\sigma}{r_c}\right)^{6}\right] & \text{for } r \le r_c \\ 0 & \text{for } r > r_c \end{cases} \tag{2}$$

where $\varepsilon = k_BT$, $r_c/\sigma = 2^{1/6}$, and σ is the size of a bead. For this form of the pairwise potential, one can calculate the corresponding second virial coefficient of beads, $B_{\mathrm{LJ}} = 2.2\sigma^3$. By equating this value to that for neutral hard spheres,[58] $B_{\mathrm{LJ}} = 2\pi d^3/3$, one finds $d = 1.02\sigma$, which we use as an estimate for the thickness (diameter) of the chain.

To simulate semiflexible chains, and to control their chain stiffness, we use an angle potential of the form

$$U_{\mathrm{angle}} = k[1 - \cos\theta_i] \tag{3}$$

where the tunable parameter k is a bending constant expressed in units of ε. The angle between adjacent bonds is equal to $\theta_i = \angle(\mathbf{u}_{i-1}; \mathbf{u}_i)$, where $\mathbf{u}_i$ is the unit bond vector connecting the i and $i+1$ monomers.[59] Increasing chain stiffness leads to an increasing Kuhn segment length l, which can be calculated as follows[60]

$$l = \frac{1 + \coth(k) - k^{-1}}{1 - \coth(k) + k^{-1}} b \approx \begin{cases} b, & k \ll 1 \\ 2kb, & k \gg 1 \end{cases} \tag{4}$$

where b is the bond length. For our model, we found that $b = 0.968\sigma$. Note that, for low $k \ll 1$, this formula neglects the (moderate) additional stiffening induced by local short-range repulsive interactions, but the system remains isotropic for low k. In contrast, at $k \gg 1$, when the stiffness is sufficiently high to induce LCO, eq 4 is rather precise. In what follows, the stiffness of the chains is quantified by the ratio $l/d \approx l/\sigma$ between the chain Kuhn segment length and the chain diameter, which is a measure of the local polymer anisodiametry (inequality of the characteristic sizes along different axes).[35]

Coulomb interactions between charged beads are given by

$$\frac{U_{\mathrm{coul}}}{k_BT} = \frac{z_i z_j l_B}{r} \tag{5}$$

where z_i is the charge valence for species i ($z_i = \pm 1$). We consider Bjerrum length values equal to $l_B = 3\sigma$ and $l_B = 5\sigma$, respectively. Long-range Coulomb interactions are calculated via the particle–particle particle–mesh (PPPM) method using LAMMPS.[61,62] The targeted error for the long-range part of the PPPM method is set to 10^{-4}. The velocities and positions of particles are updated using the velocity-Verlet algorithm with a timestep of $0.005\tau_{\mathrm{LJ}}$, where $\tau_{\mathrm{LJ}} = \sigma(m/k_BT)^{1/2}$ and m is the particle mass.

The number density of polymer beads within the coacervate is denoted by ρ. We further define the equilibrium volume fraction

$$\phi = \frac{\pi}{4} d^2 b \rho = \frac{\pi}{4} \rho \sigma^3 \tag{6}$$

of the salt-free coacervate. Here, each monomer is considered to be a cylinder of diameter d and height b. In what follows, we preferentially use volume fraction ϕ, which is the function of the number density ρ. We simulate the salt-free coacervate in the NPT ensemble with zero external pressure, $P = 0$, to mimic the coexistence of the coacervate in equilibrium with a highly dilute supernatant phase.[27,63] We use a cubic simulation box with periodic boundary conditions. The external pressure is maintained through a Berendsen barostat, and constant temperature T is maintained by coupling the system to a Langevin thermostat with damping parameter $\Gamma = 1.0m/\tau_{\mathrm{LJ}}$.[27,63]

Nematic ordering within the system is measured through the orientation order parameter S: $S = 0$ in the isotropic state and $S \to 1$ in the ideally ordered state. S is the largest eigenvalue of the orientational (order parameter) tensor Q, whose elements are given by

$$Q_{\alpha\beta} = \frac{1}{\mathcal{N}_c(N-1)} \sum_{m=1}^{\mathcal{N}_c} \sum_{i=1}^{(N-1)} \frac{1}{2}(3\mathbf{u}_{i,m}^{\alpha}\mathbf{u}_{i,m}^{\beta} - \delta_{\alpha\beta}) \tag{7}$$

where $\mathcal{N}_c$ is the number of polymer chains and N is the chain length. Here, $\mathbf{u}_{i,m}^{\alpha}$ and $\mathbf{u}_{i,m}^{\beta}$ denote the α-th and β-th components of the unit bond vector $\mathbf{u}_i$ connecting the i and $i+1$ monomers of the m-th chain; $\delta_{\alpha\beta} = 1$, if $\alpha = \beta$ while $\delta_{\alpha\beta} = 0$ if $\alpha \neq \beta$.[64] For the symmetric coacervate, we calculate the Q tensor and the resulting order parameter S via a sum over all (semiflexible) chains, as suggested by eq 7. For asymmetric coacervates, Q and S are calculated separately for flexible polycations and semiflexible polyanions.

All simulations are initialized by generating either polymer chains as self-avoiding random walks, or by using a previously obtained nematic state as the initial configuration. Equilibrium is ensured by monitoring the convergence of the coacervate density and the order parameter and by the decay of the end-to-end vector autocorrelation function as a function of simulation time.[27,63] Block averaging is performed after the system relaxes to the equilibrium. The OVITO package[65] is used to visualize the results of simulations.

https://doi.org/10.1021/acs.macromol.2c01674
Macromolecules XXXX, XXX, XXX−XXX

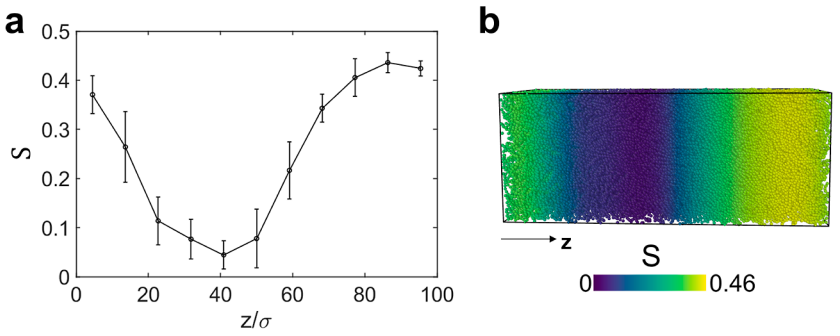

Figure 2. (a) Average order parameter S as a function of the z-axis position from NVT ensemble simulations of oppositely charged polymers. Average values are calculated by block averaging S for each sub-region of the simulation box (evenly divided the box along z axis). (b) Configuration of the system where each monomer is colored by the value of S at its location along the z axis. Simulation parameters are as follows: $f_+ = f_- = 1.0$, $l_B/\sigma = 3$, chain length $N = 20$, number of chains $\mathcal{N}_c = 2880$, and box size $X/\sigma = Y/\sigma = 40$, $Z/\sigma = 100$.

3. RESULTS AND DISCUSSION

3.1. Symmetric Coacervates of Semiflexible Polyelectrolytes. To characterize the isotropic−nematic (I−N) phase transition in salt-free coacervates, we start with a symmetric system of semiflexible polycations and polyanions of equal stiffness, that is, equal bending constants k. This system is similar to a neutral semidilute solution of semiflexible polymers, but the chains also interact via long-range Coulombic forces. We consider fully charged chains, $f_+ = f_- = f = 1$, of $N = 20$ monomers. The chain length choice was motivated by the limitations imposed by our computational resources. Choosing longer chain lengths would require a larger simulation box, a higher number of particles, and longer simulation runs because of the increase in the relaxation time. The Bjerrum length is set to $l_B/\sigma = 3$ to ensure that (i) the system reaches equilibrium within a reasonable amount of computer time and (ii) the coacervate is sufficiently dense and hence, the bending constant l/d required for nematic phase formation is not too large. At equilibrium, owing to the system's symmetry, the orientational order parameters for polyanions and polycations are equal, that is, $S_+ = S_- = S$.

The dependence of S on chain stiffness l/d is shown in Figure 1a in blue. Increasing chain stiffness induces a transition from the isotropic to the nematic state within the complex coacervate. At $l/d = 18$, the orientational order parameter S increases from 0 to 0.4 in a jump-like manner, which is indicative of a first-order phase transition. As in refs 40 and 66, we do not observe the coexistence of isotropic and nematic phases at the transition. In Figure S1 of the Supporting Information (SI), we evenly divide the simulation box into 8 cubic sub-regions, labeled with index $i = 1, 2, \cdots, 8$, and measure the order parameter S_i for each sub-region i for three different values of l/d near the transition point. These results show that, for each l/d, the values of S_i are independent of the sub-region number i. Therefore, all parts of the system exhibit an identical order and there are no signatures of a phase coexistence region in the system. To study whether a hysteresis occurs in these systems, we also performed simulations starting from two different configurations, the isotropic state with random chain orientations, and an ordered nematic state. Figure S2 in the Supporting Information shows that the sharp transition happens at almost the same values of l/d in both cases.

A coexistence region (nematic to isotropic) is absent because the coacervate corresponds to a system under a constant external pressure (NPT ensemble), rather than constant volume (NVT ensemble). In the latter case, the I−N phase coexistence always accompanies this first-order phase transition.[35] To corroborate that, we additionally performed NVT simulations of the system at the transition point, for $l/d = 18$. The total polymer density was chosen to be $\phi \approx 0.283$, which is a condition between the isotropic and nematic states observed in NPT simulations near the transition, $\phi_I = 0.278$ and $\phi_N = 0.289$. Figures 2 and S3 of the Supporting Information demonstrate the anticipated 2-phase state within the coexisting nematic and isotropic phases of our oppositely charged PEs in the NVT ensemble.

The internal structures of the isotropic and nematic coacervate phases are shown in Figure 1b. For $l/d = 1$, the system is homogeneous and isotropic, and no orientation order of PE chains is observed. For $l/d = 57$, stiff, almost perfectly rod-like PE chains are parallel to each other, but no long-range translational order is detected, which is indicative of a nematic liquid crystal.

3.1.1. Isotropic-to-Nematic Transition in the Corresponding Neutral Solution. The observed I−N transition in coacervates of semiflexible PEs induced by stiffness is predicted by theory[48,49] and resembles that encountered in neutral semidilute solutions of semiflexible polymers.[35,38,40,66−70] The only difference between salt-free coacervates and neutral semidilute solutions is the presence of electrostatic interactions. To elucidate their role in the I−N transition, we performed simulations of the corresponding solution of neutral semiflexible polymers. To this end, we first obtain equilibrium density ϕ of the salt-free coacervate formed by semiflexible PEs for each value of l/d. Then, for each value of l/d, we run NVT simulations of semidilute solutions of neutral semiflexible polymers of the same stiffness (i.e., equal k value) at the same density ϕ. The neutral solution corresponds exactly to the salt-free coacervate with Coulomb interactions turned off.

The procedure outlined above was repeated for a series of l/dvalues; the corresponding order parameters for the neutral semidilute solutions are shown in Figure 1a in black. As expected, the neutral semidilute solutions undergo an I−N first-order phase transition at increasing values of l/d.[38,71] In addition, the coexistence of two phases is also supported by the hysteresis observed in these NVT simulations, which is highlighted in Figure S4; for these simulation runs, the neutral system was initialized either from a random state or an ordered state.[72] At the transition point given by $l/d = 41$, the density of the system is equal to $\phi = 0.33$. One can also find that, at the

https://doi.org/10.1021/acs.macromol.2c01674
Macromolecules XXXX, XXX, XXX−XXX

transition, the dimensionless parameters that define its position are

$$\frac{l}{d}\phi = 13.5 \tag{8}$$

or equivalently

$$\frac{L}{d}\phi = 6.6 \tag{9}$$

Here, the value of the polymer contour length that was used is $L/d \approx N = 20$.

While in simulations of neutral persistent chains, molecules adopt almost ideal rod-like conformations and $L < l$, their flexibility is important. We find that the position of the transition differs considerably from the Onsager prediction for ideal stiff rods.[73] Within the Onsager model, the position of the spinodal

$$\left(\frac{L}{d}\phi\right)_{\text{rod}} = 4 \tag{10}$$

depends on the rod length L, and the transition takes place near the spinodal.[74] Onsager's value differs substantially from that found in simulations and given by eq 9. Furthermore, the observed value of the order parameter S at the nematic phase at the transition, $S = 0.53$, is substantially lower than that expected from the Onsager model, namely, $S_{\text{rod}} = 0.84$.

In contrast, our results are much closer to those for long polymer chains with persistent semiflexibility.[35,67] For solutions of infinitely long persistent chains, $L \gg l$, the isotropic state becomes unstable when the Kuhn segment length is sufficiently high[67]

$$\left(\frac{l}{d}\phi\right)_{\text{pers},N\to\infty} = 12 \tag{11}$$

and, at the transition, the order parameter in the nematic phase equals $S_{\text{pers}} = 0.49$. This good agreement between eqs 8 and 11 is also consistent with the results of Khokhlov and Semenov,[67] who predicted that even short persistent chains with a contour length as low as $L \approx 0.5l$ are much more akin to long persistent chains rather than short, ideally stiff Onsager rods.[67] This effect has been attributed to the role of chain ends. In persistent chains, due to the underlying bending fluctuations, the ends are much less aligned than the middle monomers, even for $L < l$. The Onsager theory of perfectly stiff rods predicts much easier and stronger ordering (i.e., a lower l/d transition value and a higher order parameter, S, in the nematic phase) and is inaccurate because it neglects these orientation fluctuations of the polymer ends.[67]

The following spinodal found by Khokhlov and Semenov in ref 67

$$\frac{L}{d}\phi = \frac{12L/l}{1 - \frac{1-\exp(-6L/l)}{6L/l}} \tag{12}$$

unifies the limiting cases of Onsager's rods and long persistent chains. It reproduces eq 10 for ideally stiff rods, $L \ll l$, and eq 11 for long persistent polymers, $L \gg l$. Substituting the parameters of our system at the transition, $L/\sigma = 20$ and $l/\sigma = 40$, in the rhs of this interpolating formula, one finds $\phi L/d = 8.8$, which is somewhat above the observed value of $\phi L/d = 6.6$. Equation 12 overestimates the spinodal value of L/d because it is based on the Onsager approach to anisotropic excluded volume interactions that considers only pairwise repulsions between polymer statistical segments. As any virial expansion, it is limited to low density solutions, $\phi \ll 1$. The density of the studied solution at the I–N transition is relatively large, $\phi = 0.33$, and higher order (at least three-body) contributions become significant.

Onsager's approach to anisotropic repulsive interactions can be systematically generalized to dense polymer solutions by decoupling translational and orientational degrees of freedom. The latter enable the density-dependent renormalization of the second virial coefficient of anisotropic interactions between statistical segments:[35,69,70,75]

$$B(\gamma) = 2l^2 d \sin\gamma \rightarrow \tilde{B}(\gamma, \phi) = 2l^2 d \frac{|\ln(1-\phi)|}{\phi}\sin\gamma \tag{13}$$

where γ is the angle between interacting segments. The Onsager second virial coefficient is reproduced at low densities, $\tilde{B}(\gamma, \phi) \approx B(\gamma)$ for $\phi \ll 1$. After this renormalization, the modified spinodal, which is an extension of eq 12 for dense solutions, reads

$$\frac{L}{d}\phi = \frac{12L/l}{1 - \frac{1-\exp(-6L/l)}{6L/l}} \times \frac{\phi}{|\ln(1-\phi)|} \tag{14}$$

Subsisting $L/l = 0.5$ and $\phi = 0.33$, one finds that the prediction of this modified spinodal, $L\phi/d = 7.3$, is remarkably close to the value observed in simulations, $L\phi/d = 6.6$.

To recapitulate, if we had used much shorter chains, the simulation results would have become closer to the predictions of the Onsager theory for rod-like polymers, which is accurate at $L \ll l$. On the contrary, for much higher N values providing $L \gg l$, simulation results are expected to better agree with the theoretical predictions for long persistent chains. In the case of intermediate chain lengths considered in this work, the unifying formula given by eq 14 should be used to accurately predict the spinodal of the I–N transition.

3.1.2. Comparison between Neutral and Charged Systems. We now return to the I–N transition in the complex coacervate. Compared to the corresponding neutral systems, the coacervate becomes liquid crystalline at substantially lower magnitudes of the chain stiffness. The threshold values differ more than twice, $(l/d)_{\text{coac}} = 18$ versus $(l/d)_{\text{neut}} = 41$, as seen in Figure 1a. This result is consistent with earlier theoretical works,[48,49] which predicted that anisotropic Coulomb interactions between semiflexible PEs facilitate nematic ordering in coacervates.

The dependence of the coacervate density on PE stiffness is shown in Figure 3. The vertical dash line given by $l/d = 18$ delineates the isotropic and nematic coacervate states. The coacervate density is a non-monotonic function of l/d, which decreases when the coacervate is isotropic and increases when it is nematic. For isotropic coacervates, a similar decrease in the density has been recently reported in ref 50. This can be primarily attributed to the increasing strength of excluded volume interactions between randomly oriented segments/rods, that is, the increase in the second virial coefficient given by eq 13, $B \sim l^2$. Additionally, higher values of l/d lead to effectively lower local fractal dimensions of the PEs (their conformations) and hence weaker Coulomb correlation attractions.[49,76] At the I–N transition, the nematic ordering of PEs reduces their excluded volume repulsions and enhances their Coulomb attractions,[48,49] leading to a sudden growth of

https://doi.org/10.1021/acs.macromol.2c01674
Macromolecules XXXX, XXX, XXX−XXX

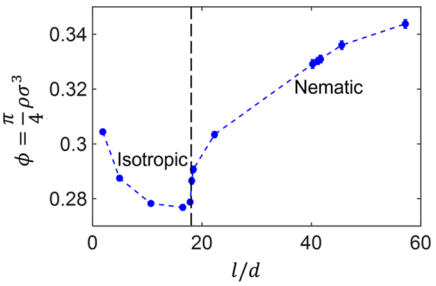

Figure 3. Dependence of coacervate volume fraction ϕ on chain stiffness l/d. The black dash line indicates the approximate position of the transition between the isotropic and nematic states. Simulation parameters: $f_+ = f_- = 1.0$, $l_B/\sigma = 3$.

the coacervate density. (In a similar way, the nematic phase in solutions of neutral semiflexible polymers is always denser than the coexisting isotropic phase.[35,40,66,77,78]) Finally, in the nematic coacervate, an increase in the PE stiffness improves alignment of the chains. The growth of the order parameter shown in Figure 1a, from $S = 0.53$ at the transition to $S \approx 0.8$ for $l/d \geq 40$, results in decreasing steric repulsions and increasing electrostatic attractions,[48,49,79,80] thereby increasing the density of the LC coacervate.

The observations above demonstrate the effect that Coulomb interactions have on the macroscopic phase behavior of coacervates. However, the results shown in Figure 1 do not allow us to separate contributions due to (i) the electrostatic stiffening of PEs[81−85] and (ii) the bare anisotropic, orientation-dependent Coulomb interactions.[48,49,79,80] We emphasize that the former effect facilitates nematic order indirectly, through the renormalization of the net polyion stiffness. This effect has been neglected in past theoretical considerations of LC phases of semiflexible PEs, which mostly deal with perfectly stiff, rod-like chains. In contrast, theoretical models[48,49,79,80] predict a strong role for the second factor. It is therefore of interest to examine these predictions more rigorously by untangling contributions (i) and (ii).

In our simulations, we can consider the conformational statistics of each PE within the coacervate phase. To this end, we again compare complex coacervates and neutral semidilute solutions of equal density, but now we match chain conformations, as opposed to only non-electrostatic contributions due to the chain stiffness, l/d. We emphasize that conformations are a representative of the net persistent length of the chains, which for PEs includes two terms, $l_{tot} = l_0 + l_{el-st}$. Here, l_0 is the "bare" stiffness of the polymer in the absence of Coulomb interactions, which is defined by the bending constant k in the angle potential of eq 4, and l_{el-st} represents the electrostatic stiffening.[81−85]

The comparison procedure is as follows. For the coacervate simulations at a given bare stiffness of the PEs, $l_0/d = (l/d)_{coac}$, we calculate the mean-square internal distance $\langle R^2(n)\rangle$. Then, simulations of the neutral solution of equal density are performed and the stiffness of the neutral chains $l_{tot}/d = (l/d)_{neut}$ is adjusted to provide a $\langle R^2(n)\rangle$ that coincides with that of the PEs within the coacervate. One can expect $(l/d)_{neut} > (l/d)_{coac}$, and the difference between these values corresponds to the effective electrostatic persistent length of the PEs within the coacervate

$$\frac{l_{el-st}}{d} = \frac{l_{tot} - l_0}{d} = \left(\frac{l}{d}\right)_{neut} - \left(\frac{l}{d}\right)_{coac} \quad (15)$$

An example that illustrates this procedure is provided in Figure 4a. The polymer statistics in the neutral semidilute solution at $(l/d)_{neut} = 22.3$ are very close to those of PEs in the coacervate at $(l/d)_{coac} = 17.4$, as evidenced by the agreement between the blue and black curves. The process of matching neutral and charged polymer chains was performed over a wide range of chain stiffness $(l/d)_{coac}$, and the results are summarized in Figure 4b. Here, each point corresponds to a pair of values, $((l/d)_{coac}; (l/d)_{neut})$. The vertical and horizontal dashed lines, given by $(l/d)_{coac} = 18$ and $(l/d)_{neut} = 41$, denote the transition between the isotropic and nematic states in the coacervate and in the corresponding neutral solution, respectively. We emphasize that the horizontal dashed line intersects the obtained curve at $(l/d)_{coac} \approx 21$, which is noticeably higher than the transition value for the coacervate, $(l/d)_{coac} = 18$. That is, at $18 < (l/d)_{coac} < 21$ the coacervate is a nematic LC, but the respective neutral solution of the same density and the same net polymer stiffness remains isotropic. This result serves to clarify the role of factor (ii), and it proves that anisotropic Coulomb interactions between stiff/semi-flexible PEs enhance their orientational order, as expected theoretically.[48,49,79,80]

The red straight line in Figure 4b is given by $(l/d)_{coac} = (l/d)_{neut}$, and it corresponds to the equality between

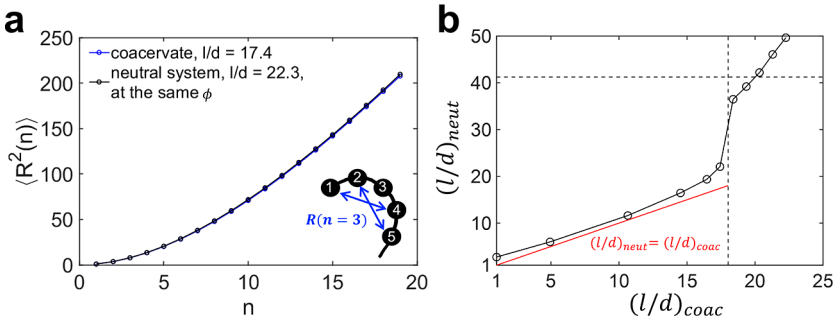

Figure 4. (a) Mean-squared internal distance $\langle R^2(n)\rangle$ of PE chains in the salt-free coacervate (blue) and for neutral polymers in the respective semidilute solution with the same polymer volume fraction, ϕ (black). The schematic illustrates the value of $\langle R^2(n)\rangle$ for $n = 3$. (b) Dependence of chain stiffness in neutral semidilute solutions, $(l/d)_{neut}$, on the bare stiffness of PEs in the complex coacervate, $(l/d)_{coac}$. Neutral solutions and coacervates have equal densities and identical chain conformational statistics. The red solid line is given by $(l/d)_{coac} = (l/d)_{neut}$, and the vertical and horizontal dash lines denote the positions of I−N transitions in coacervates and neutral solutions, respectively. The simulation parameters are $f_+ = f_- = 1.0$ and $l_B/\sigma = 3$.

https://doi.org/10.1021/acs.macromol.2c01674
Macromolecules XXXX, XXX, XXX−XXX

bare and net persistent length, $l_{tot} = l_0$. Below the I−N transition point, the black curve is only slightly above this straight red line, indicating minor contributions from the electrostatic stiffening[81−85] to the net persistent length of the PEs. The strong growth in the apparent persistent length at $(l/d)_{coac} > 18$ is due to the orientation order of the PEs. (We recall that, for $18 < (l/d)_{coac} < 21$, their conformations are comparable to those of the neutral polymers in the isotropic solution).

Another way to highlight the role of Coulomb interactions in the intracoacervate LC order is to compare the position of I−N transition across coacervates of PEs with different fractions of ionic monomers. We consider systems with a fixed value of $f_- = 1.0$, and a series of f_+ equal to 1.0, 0.75, 0.6, 0.55, and 0.5, with the charged/neutral monomers spaced in the polycations as evenly as possible to minimize the effect of sequence.[86] To separate the contributions due to Coulomb and excluded volume interactions, the coacervates are compared to the respective neutral semidilute solutions of equal density. The dependence of the order parameter S on the bending constant k is shown in Figure 1a for $f_+ = 1.0$ and in Figure S5 of Supporting Information for $f_+ = 0.75$ and 0.5. To quantify the I−N transition, we use the value of the chain stiffness at the transition, l/d, which corresponds to a sharp increase of the order parameter, S.

Figure 5 shows the transition values of l/d plotted as a function of f_+. The blue and black curves correspond to coacervates and neutral solutions, respectively. The black curve represents the position of the I−N transition in the absence of Coulomb forces, when LC ordering is driven solely by excluded volume interactions. Two conclusions can be drawn on the basis of the results in Figure 5. First, electrostatic interactions facilitate the phase transition because the threshold stiffness l/d is always lower in their presence (the blue curve is below the black one). Second, the difference between the threshold l/d values goes down as f_+ increases. This effect has been theoretically predicted in our earlier work, ref 49, for asymmetric semiflexible−flexible coacervates (see Figure 9 therein) and can be explained as follows. The high charge density of PEs results in a high coacervate density. Coulomb interactions play a dominant role in the LC order at low coacervate densities, while, in dense coacervate phases, excluded volume interactions are the key factor for the nematic phase formation.[49] For this reason, the values of l/d for coacervates and for neutral solutions are the closest when the polycation ionization is the highest, $f_+ = 1$.

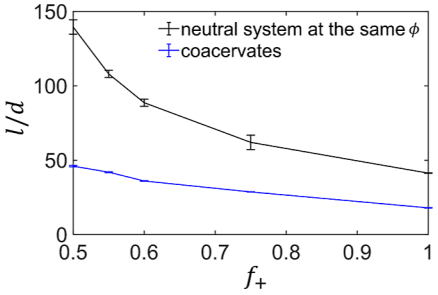

Figure 5. Dependence of the stiffness l/d at the I−N transition on the charge fraction of polycations f_+ for salt-free coacervates (blue), and the corresponding solutions of neutral polymers with equal volume fraction ϕ (black). The error bar indicates the estimated range of l/d values at the transition from the isotropic state to the nematic state (corresponding to a sudden increase of the order parameter S). The simulation parameters are as follows: $f_- = 1.0$, $l_B/\sigma = 3$, and $N = 20$.

While the predictions of the RPA theory[48,49] and our simulations are consistent with each other, the agreement is not quantitative. For example, one can consider the symmetric coacervate with $f_+ = f_- = f$. Following the analysis for neutral solutions performed in Subsection 3.1.1, it is reasonable to approximate PEs as long persistent chains. In this case, the resulting spinodal can be written as[49]

$$\frac{l}{d}\phi = \frac{12}{1 + \frac{\pi f^2 l_B}{3\phi d}} \tag{16}$$

and the second term in the denominator quantifies the relative importance of Coulomb interactions in inducing LCO. When it is much lower than unity, excluded volume interactions dominate, and eq 16 reduces to the result for neutral persistent chains, eq 11. In contrast, at $\pi f^2 l_B/3\phi d \gg 1$, Coulomb interactions are dominant. Substituting $l_B/d \approx l_B/\sigma = 3$ and $f_+ = f_- = 1$ into the rhs of eq 16, we find that the theoretical prediction, $l\phi/d = 0.98$, differs drastically from the simulated value of the lhs at the I−N transition for the coacervate, $l\phi/d = 5.04$. Because the agreement for neutral chains was reasonable, this mismatch highlights that the RPA-based theory strongly overestimates the role of Coulomb interactions. Another way to see this is to calculate $\pi f^2 l_B/3\phi d \approx 11 \gg 1$. In fact, this parameter should be on the order of unity because the l/d value for coacervates with $f_+ = f_- = 1$ differs from that for the respective neutral solutions by only a factor of two.

This discrepancy can be attributed to the limited applicability range of theories based on the RPA, which are only justified for weakly charged coacervates,[48,49] $f^2 l_B/d \ll 1$. In contrast, simulations are performed at high Bjerrum lengths, $l_B/d \approx 3$, and high PE ionizations, $f = 1$, which represent the fully charged homoPEs that are studied in experiments, when correlations are strong. To quantitatively corroborate the theoretical predictions of ref 49 and access intra-coacervate LC ordering at low f and l_B values, simulations of much longer chains are required. The latter are computationally demanding. To quantitatively match the simulation results presented here, the RPA-based theory of refs 48 and 49 should be extended to include strong charge correlations. This can be potentially achieved by following the method of our recent work,[87] namely, by taking into account the discreteness of charges in PEs[80] and the finite number of fluctuation wave modes in the system.[88] The second aspect appears particularly important for stiff PEs with rigidly connected neighboring charges that have no independent translational degrees of freedom,[87] and neglecting it may be the primary reason behind the standard RPA's limitations.

3.2. Asymmetric Coacervates of Semiflexible Polyanions and Flexible Polycations. In this subsection, we consider coacervates with a stiffness asymmetry, formed from semiflexible polyanions and flexible polycations. These systems represent a minimal model of coacervates formed from dsDNA and a flexible, oppositely charged polyanions such as PLL. Such systems have been studied in recent experiments.[43] An additional motivation to simulate these coacervates is a desire to test several theoretical assumptions and conclusions from our recent work, ref 49.

The simulation setup and procedure are similar to those mentioned in Subsection 3.1, except that an angle potential is only used for polyanion chains. We first calculate the order

https://doi.org/10.1021/acs.macromol.2c01674
Macromolecules XXXX, XXX, XXX−XXX

parameter S_- only for the polyanions to quantify the nematic order in the coacervate. These results are shown in Figure 6.

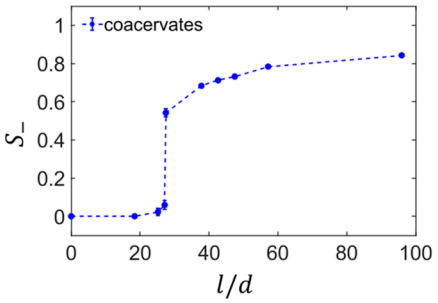

Figure 6. Dependence of the order parameter S_- for semiflexible polyanions on their stiffness l/d for salt-free coacervates. The simulation parameters are $f_+ = f_- = 1.0$ and $l_B/\sigma = 5$.

Here, we use a larger Bjerrum length, $l_B/\sigma = 5$ instead of the $l_B/\sigma = 3$ value that was used for stiffness-symmetric coacervates in Subsection 3.1; we do so to provide easier access to low values of f_+, which we consider in what follows.

The observed I−N transition, which is accompanied by a sudden change in S_-, has been theoretically predicted.[49] Note that previous theoretical works neglected the ordering of flexible polycations and assumed $S_+ = 0$ both below and above the transition. We examine this assumption by calculating the nematic order parameter S_+ for flexible polycations. The results for S_- and S_+ for two coacervate systems, one with $f_- = f_+ = 1.0$ and another with $f_- = 1.0$, $f_+ = 0.5$, are shown in Figure 7. One can see that the I−N transition in complex coacervates is accompanied by a weak ordering of the flexible polycations, with the corresponding order parameter S_+ being in the range of 0.15−0.2. We emphasize that S_+ is approximately 4 times lower than the corresponding value S_- for semiflexible polycations, which makes the theoretical assumption of ref 49 reasonable, though not quantitative. The nematic ordering of flexible polycations is induced by the strong ordering of the semiflexible polyanions and the Coulomb attractions between oppositely charged PEs. The role of the second factor can be clearly seen by comparing the results in Figure 7a,b. As f_+ decreases from 1 to 0.5 and electrostatic attractions weaken, the order parameter S_+ for flexible chains decreases from around 0.2 to 0.1, while the value of S_- remains almost unchanged. Hence, one can expect that, for PEs with low charge densities, $f_\pm \ll 1$, which we considered in ref 49, S_+ should be sufficiently close to zero.

Also note that a similar ordering of flexible chains induced by the ordering of stiff chains has been reported in simulations of mixtures of neutral amphiphilic polymers with different stiffness,[89] although attractions between the polymers of various types were induced by poor solvent conditions, rather than Coulomb interactions between them.

For stiffness-asymmetric coacervates, separating the roles of Coulomb and excluded volume interactions is more challenging because a direct comparison of results for coacervates with those for neutral semidilute solutions is not always possible. This arises because, in mixed neutral solutions, flexible and semiflexible chains are prone to segregation from each other, forming two coexisting macroscopic phases, one isotropic and one nematic. For this reason, we were unable to perform a comparison of the coacervate with $f_+ = f_- = 1$ to the respective neutral solution. The latter does not remain in one phase, and the corresponding order parameter for the homogeneous neutral solution (shown in Figure 1 for the stiffness-symmetric system with the black curve) cannot be added to Figure 6.

Figure 8 shows that the same effect takes place for the neutral solution corresponding to the stiffness-asymmetric coacervate with $f_- = 1$ and $f_+ = 0.5$. For $f_- = 1$ and $f_+ = 0.5$, simulation configurations of the uniphase complex coacervate and the respective phase-separated neutral solution are shown in Figure 8b. One can clearly see two coexisting domains (phases), rich in flexible (red) chains and semiflexible (blue) chains. The nematic phase has a lower volume because of the higher density and the stoichiometry of the reference coacervate: there are twice as many flexible chains than semiflexible chains in the system. To confirm the phase separation of the mixed solution of neutral flexible and semiflexible chains, the cubic simulation box was divided into 8 cubic sub-boxes, and the nematic order parameter S_- was calculated for each of them. Note that, for the neutral system, S_- denotes the order parameter for semiflexible chains. The dependence of S_-^i on the sub-box number i is shown in Figure 8a and demonstrates that the coacervate remains homogeneous, while the respective neutral system is phase separated. For the latter case, the nematic order parameter is high in the phase rich in semiflexible chains and close to zero for the coexisting phase, which consists predominantly of flexible polymers. For mixed solutions of neutral polymers of different stiffness, a similar demixing transition has also been reported by our group and by others in theoretical studies,[90,91] Monte Carlo[72,91−94] and MD simulations.[95−97]

The effective short-range incompatibility between flexible and semiflexible polymers, which is induced by the stiffness

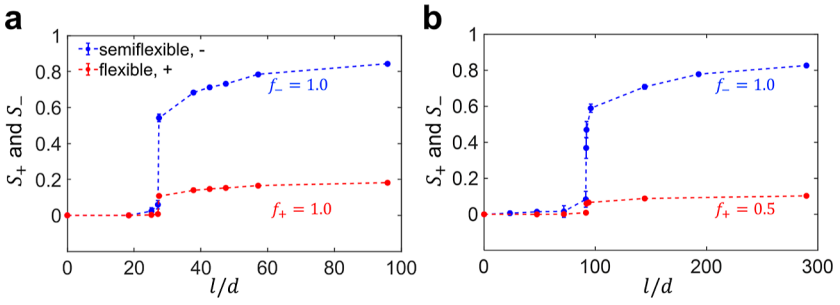

Figure 7. Dependence of the order parameters S_- and S_+ for semiflexible polyanions (blue curve) and flexible polycations (red curve), respectively, on polyanion stiffness l/d in salt-free coacervates with different polycation charge densities: (a) $f_+ = 1.0$ and (b) $f_+ = 0.5$. Other simulation parameters are $f_- = 1.0$ and $l_B/\sigma = 5$ for both plots.

https://doi.org/10.1021/acs.macromol.2c01674
Macromolecules XXXX, XXX, XXX−XXX

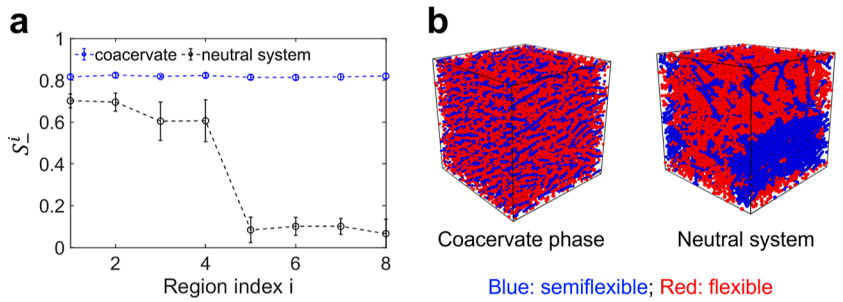

Figure 8. (a) Order parameter S^i_- for semiflexible chains in each cubic sub-region of the simulation box as a function of the region index i for the salt-free coacervate at l/d = 289 (blue symbols) and the corresponding neutral system of the equal density (block symbols) and (b) simulation configurations of these coacervate and neutral systems. Semiflexible and flexible chains—PEs in coacervate and non-ionic polymers in the neutral system—are shown in blue and red, respectively. The simulation parameters are f_+ = 0.5, f_- = 1.0, and l_B/σ = 5.

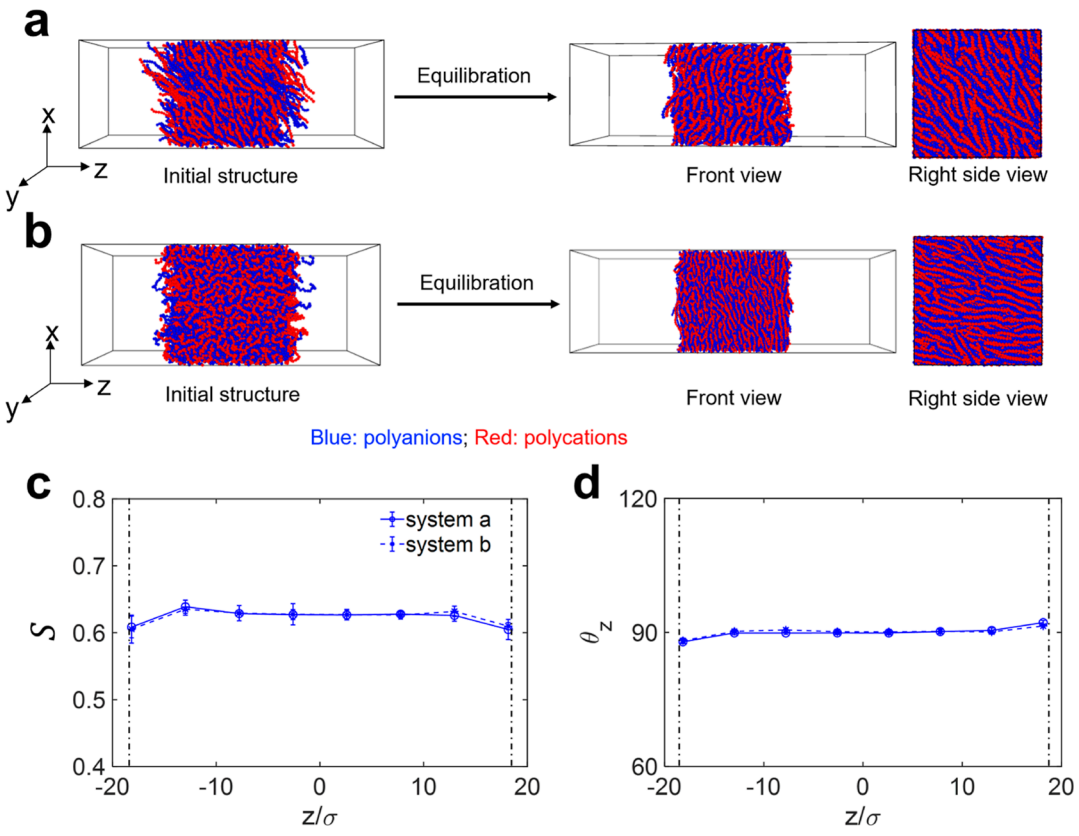

Figure 9. Simulation visualization of the interface between a nematic coacervate phase formed from semiflexible PEs with l/d = 22 and the supernatant. Figures (a,b) correspond to simulations started from nematic (equilibrium) and isotropic (non-equilibrium) initial states of the coacervate phase, respectively. Polyanions and polycations are shown in blue and red, and the simulation parameters are $f_+ = f_-$ = 1.0 and l_B/σ = 3. Average values of (c) order parameter S and (d) angle θ_z between bond vectors and the z-axis, along the z-axis, are plotted for systems shown in (a,b) at equilibrium. The center of mass of the coacervate phase is chosen as the origin of the Cartesian coordinate. The two dash-dotted lines in (c,d) mark the boundaries of coacervate phases.

mismatch, does not manifest itself in the complex coacervate (see Figure 7b). This is due to the strong Coulomb attractions between oppositely charged PEs, which overcome the weak short-range repulsions. Generally speaking, the formation of a microphase-separated complex coacervate can be expected provided that (i) the difference in the stiffness of the PEs is high and (ii) the fraction of ionic monomers in the PEs is very low, $f_\pm \ll 1$. The latter provides a low Coulomb energy for the charge-imbalanced oppositely charged domains rich in polyanions and polycations. This type of electrostatically stabilized microphase separation has been recently studied in coacervates/blends of flexible but chemically incompatible PEs.[31,32,98−100] For the mixture of PEs with unequal stiffness, the only difference is the orientational order inside the domains: polyanion-rich domains may be nematic, while polycation-rich domains remain isotropic.

3.3. Interfacial Orientational Ordering in Nematic Coacervates. Subsections 3.1 and 3.2 were devoted to a characterization of the macroscopic phase behavior of complex coacervates and the role of Coulomb interactions in such systems. In this subsection, we consider the interfacial properties of nematic coacervates and focus on the chains' orientation at the coacervate-supernatant interface—a phe-

https://doi.org/10.1021/acs.macromol.2c01674
Macromolecules XXXX, XXX, XXX−XXX

nomenon referred to as anchoring in the liquid crystal literature.

We consider a stiffness-symmetric complex coacervate, which was discussed in Subsection 3.1 and Figure 1. At l/d = 22 this coacervate is nematic, as was found in NPT simulations. We now perform direct NVT simulations of coexistence between the coacervate and the supernatant phases. The configuration of the nematic coacervate obtained in NPT simulations is inserted inside an empty elongated cuboid box of the same cross-section, as shown in Figure 9a. The axis parallel to the longest cuboid size is denoted by z.

Simulations are then performed in the NVT ensemble with periodic boundary conditions; the solvent is included implicitly. This setup enables consideration of the coacervate film between two coacervate−supernatant interfaces, which are approximately perpendicular to the z-axis.

After equilibration, the coacervate phase remains nematic (as shown in Figure 9c), and its density is unchanged, as expected. Snapshots in Figure 9a show that, at equilibrium, the PEs align parallel to the coacervate−supernatant interface, that is, they exhibit homogeneous alignment. The front view demonstrates that very few chain ends protrude from the coacervate into the supernatant, and the interface is flat, with some deviations due to thermal fluctuations and the low coacervate−supernatant interfacial tension. On the rhs view, one can see that chains at the interface lie parallel to it, in spite of the fact that they had a different relative orientation in the initial configuration of the system.

To quantify the interfacial ordering of the semiflexible PEs, we calculated the nematic order parameter that characterizes the ordering along the z-axis, that is, perpendicular to the coacervate−supernatant interface

$$S_z = Q_{zz} = \frac{3\langle \cos^2 \theta_z \rangle - 1}{2} \tag{17}$$

Here θ_z is the angle between the bond direction and the z-axis. The distribution of θ_z along z-axis is plotted in Figure 9d. The resulting average value of S_z = −0.33 within the coacervate phase supports our conclusions, as seen in Figure S6 of Supporting Information. (Recall that S_z = −0.5 would correspond to an ordering perfectly parallel to the OXY plane.) Additionally, it demonstrates that the film thickness is relatively low, and the preferential parallel orientation at the interface induces the same orientation inside the entire film.

To confirm this finding, we performed analogous simulations starting from another initial configuration, in which the coacervate has the same density (that of the equilibrium nematic coacervate for l/d = 22) but is isotropic. Figure 9b shows that the system relaxes to an identical equilibrium configuration, with nematic order, and homogeneous alignment of the PE chains at the interface.

For our complex coacervates, this result can be rationalized as follows. By adopting the parallel orientation, the interfacial chains can move/slide freely with respect to each other along the interface while remain inside the nematic coacervate phase. In contrast, if they were perpendicular to the interface, the relative motion of rod-like chains would result in the chains' protruding into the supernatant and a loss of electrostatic interactions with their oppositely charged counterparts, which would be energetically unfavorable. This restricted movement of the chains would result in a lower configurational (translational) entropy of a system with homeotropic (perpendicular) alignment. This entropic difference makes the in-plane, parallel orientation of PEs at the interface thermodynamically favorable. We finally note that the orientational ordering parallel to the interface has also been theoretically predicted for interfaces of coexisting nematic and isotropic phases.[101]

The planar anchoring, which was observed at the coacervate−supernatant interface, is not typical of most liquid crystals. We cannot rule out that this result could be influenced by finite-size effects; the dimensions of the macroscopic coacervate phase in the z-direction exceed the contour length of the semiflexible polyions by a factor of 2, $\Delta Z/L \approx 2$, as seen in Figure 9. We also note that the ratio of the box length to the PE length could not be sufficiently large to observe the formation of a smectic phase, which has been documented in systems of neutral stiff rods (spherocylinders)[102] and semiflexible polymers.[41] According to ref 41, a large simulation box with dimensions exceeding the chain length by an order of magnitude is needed to obtain a smectic phase in a system of neutral polymers. A more comprehensive study of interfacial chain orientation and smectic phase formation will be conducted in the future using large-scale simulations and advanced sampling techniques.

4. CONCLUSIONS

We have investigated the emergence of LCO within salt-free coacervates containing semiflexible PEs using MD simulations. PEs were represented within the Kremer−Grest model, augmented with Coulomb interactions and angle-bending potentials. The main findings of the present work can be summarized as follows:

(i) For both symmetric semiflexible−semiflexible and asymmetric semiflexible−flexible coacervates, the transition from the isotropic to the nematic state (I−N) has been observed at increasing stiffness of the semiflexible chains. This result is consistent with earlier theoretical predictions and experimental findings. The I−N transition is a first-order phase transition accompanied by a pronounced increase in the nematic order parameter S_- of the semiflexible polyanions.

(ii) For stiffness-symmetric coacervates, the density is a nonmonotonic function of the PE stiffness l/d. At low l/d, when the coacervate is isotropic, the density decreases with increasing the chain stiffness. However, at the I−N transition, the density abruptly increases and keeps growing with increasing l/d in the nematic state. This is due to the dependence of anisotropic excluded volume repulsions and anisotropic Coulomb attractions on the orientational order of the PEs, S. The higher the order parameter S, the weaker the excluded volume effects and the stronger the electrostatic attractions between the polyions.

(iii) To confirm earlier theoretical predictions concerning how Coulomb interactions facilitate intracoacervate LCO,[48,49] the coacervate phase behavior was compared with that of semidilute solutions of neutral polymers of equal density. The I−N transition in the latter systems takes place at approximately twice the value of l/d. While this effect can be partially attributed to the electrostatic stiffening of PEs, a comparison between coacervates and neutral polymer solutions of equal total stiffness demonstrates that the transition l/d value remains

https://doi.org/10.1021/acs.macromol.2c01674
Macromolecules XXXX, XXX, XXX−XXX

higher in neutral systems. This is in qualitative agreement with theoretical calculations based on the RPA.[48,49] Moreover, a comparison of the I−N transition across coacervates (and the respective neutral systems) having different ionization of polycations demonstrates that Coulomb interactions are the main trigger for the nematic ordering of coacervates with low density. In contrast, when the coacervate density is high, excluded volume interactions are the dominant driving force for the orientational order, as was anticipated by theory.[48,49]

(iv) For asymmetric semiflexible−flexible coacervates, in addition to the strong nematic ordering of semiflexible polyanions expected by theory, we also observe a weak ordering of flexible polycations, which was neglected in previous theoretical treatments.[49] As an example, for coacervates formed from fully charged PEs, we find $S_- \approx 0.6$ and $S_+ \approx 0.15$ in the ordered phase at the I−N transition. For asymmetric coacervates, we were unable to perform a comparison to neutral systems because the latter undergo a macroscopic phase separation into two phases. This phase separation is absent in coacervates because of the strong Coulomb attractions between oppositely charged PEs. This Coulomb coupling is also the reason for the weak ordering of flexible polycations that is induced by the strong polyanion ordering.

(v) Simulations have revealed a preferential, parallel ordering (planar anchoring) at the interface between the nematic coacervate and the supernatant.

The results presented here could be helpful in understanding some of the molecular mechanisms for prebiotic evolution involving dsDNA and PEs, including disordered proteins, and for inspiring new ways of designing coacervate-based materials by turning the stiffness of the underlying molecules.

■ ASSOCIATED CONTENT

Supporting Information

The Supporting Information is available free of charge at https://pubs.acs.org/doi/10.1021/acs.macromol.2c01674.

patial distribution of order parameter for salt-free coacervates formed by semiflexible PEs around transition bending constant; isotropic-to-nematic transition in salt-free coacervates formed by semiflexible PEs with different initial configurations; coexistence of the nematic and isotropic phases in the charged system with NVT ensemble simulation; isotropic-to-nematic transition for the neutral semiflexible polymer solution with different initial configurations; isotropic-to-nematic transition in salt-free coacervates formed by semiflexible PEs with different charge fractions of polycations; and nematic order parameter along the z-axis of PEs within the salt-free coacervate interfaced with the supernatant phases (PDF)

■ AUTHOR INFORMATION

Corresponding Author

Juan J. de Pablo − *Pritzker School of Molecular Engineering, University of Chicago, Chicago, Illinois 60637, United States; Center for Molecular Engineering, Argonne National Laboratory, Lemont, Illinois 60439, United States;* orcid.org/0000-0002-3526-516X; Email: depablo@uchicago.edu

Authors

Boyuan Yu − *Pritzker School of Molecular Engineering, University of Chicago, Chicago, Illinois 60637, United States;* orcid.org/0000-0002-8200-4413

Heyi Liang − *Pritzker School of Molecular Engineering, University of Chicago, Chicago, Illinois 60637, United States;* orcid.org/0000-0002-8308-3547

Artem M. Rumyantsev − *Pritzker School of Molecular Engineering, University of Chicago, Chicago, Illinois 60637, United States;* orcid.org/0000-0002-0339-2375

Complete contact information is available at: https://pubs.acs.org/10.1021/acs.macromol.2c01674

Notes

The authors declare no competing financial interest.

■ ACKNOWLEDGMENTS

Helpful discussions with Noe Atzin and Gustavo Perez-Lemus are highly acknowledged. This work was supported by the Department of Energy, Basic Energy Sciences, Division of Materials Science and Engineering.

■ REFERENCES

(1) Hyman, A. A.; Weber, C. A.; Jülicher, F. Liquid-liquid phase separation in biology. *Annu. Rev. Cell Dev. Biol.* **2014**, *30*, 39−58.

(2) Alberti, S.; Gladfelter, A.; Mittag, T. Considerations and challenges in studying liquid-liquid phase separation and biomolecular condensates. *Cell* **2019**, *176*, 419−434.

(3) Shakya, A.; Park, S.; Rana, N.; King, J. T. Liquid-liquid phase separation of histone proteins in cells: Role in chromatin organization. *Biophys. J.* **2020**, *118*, 753−764.

(4) Frankel, E. A.; Bevilacqua, P. C.; Keating, C. D. Polyamine/nucleotide coacervates provide strong compartmentalization of Mg^{2+}, nucleotides, and RNA. *Langmuir* **2016**, *32*, 2041−2049.

(5) Aumiller, W. M., Jr.; Davis, B. W.; Keating, C. D. Phase separation as a possible means of nuclear compartmentalization. *Int. Rev. Cell Mol. Biol.* **2014**, *307*, 109−149.

(6) Drobot, B.; Iglesias-Artola, J. M.; Le Vay, K.; Mayr, V.; Kar, M.; Kreysing, M.; Mutschler, H.; Tang, T.-Y. D. Compartmentalised RNA catalysis in membrane-free coacervate protocells. *Nat. Commun.* **2018**, *9*, 3643.

(7) Aumiller, W. M., Jr.; Pir Cakmak, F.; Davis, B. W.; Keating, C. D. RNA-based coacervates as a model for membraneless organelles: Formation, properties, and interfacial liposome assembly. *Langmuir* **2016**, *32*, 10042−10053.

(8) Yewdall, N. A.; André, A. A. M.; Lu, T.; Spruijt, E. Coacervates as models of membraneless organelles. *Curr. Opin. Colloid Interface Sci.* **2021**, *52*, 101416.

(9) Donau, C.; Späth, F.; Sosson, M.; Kriebisch, B. A. K.; Schnitter, F.; Tena-Solsona, M.; Kang, H.-S.; Salibi, E.; Sattler, M.; Mutschler, H.; Boekhoven, J. Active coacervate droplets as a model for membraneless organelles and protocells. *Nat. Commun.* **2020**, *11*, 5167.

(10) Uversky, V. N. Protein intrinsic disorder-based liquid-liquid phase transitions in biological systems: Complex coacervates and membrane-less organelles. *Adv. Colloid Interface Sci.* **2017**, *239*, 97−114.

(11) Jia, T. Z.; Fraccia, T. P. Liquid crystal peptide/DNA coacervates in the context of prebiotic molecular evolution. *Crystals (Basel)* **2020**, *10*, 964.

(12) Mason, A. F.; Buddingh', B. C.; Williams, D. S.; van Hest, J. C. M. Hierarchical self-assembly of a copolymer-stabilized coacervate protocell. *J. Am. Chem. Soc.* **2017**, *139*, 17309−17312.

(13) Koga, S.; Williams, D. S.; Perriman, A. W.; Mann, S. Peptide-nucleotide microdroplets as a step towards a membrane-free protocell model. *Nat. Chem.* **2011**, *3*, 720−724.

(14) Marciel, A. B.; Srivastava, S.; Tirrell, M. V. Structure and rheology of polyelectrolyte complex coacervates. *Soft Matter* **2018**, *14*, 2454−2464.
(15) Kudlay, A.; Ermoshkin, A. V.; Olvera de la Cruz, M. Complexation of oppositely charged polyelectrolytes: Effect of ion pair formation. *Macromolecules* **2004**, *37*, 9231−9241.
(16) Wang, Z.; Rubinstein, M. Regimes of conformational transitions of a diblock polyampholyte. *Macromolecules* **2006**, *39*, 5897−5912.
(17) Ou, Z.; Muthukumar, M. Entropy and enthalpy of polyelectrolyte complexation: Langevin dynamics simulations. *J. Chem. Phys.* **2006**, *124*, 154902.
(18) Lee, J.; Popov, Y. O.; Fredrickson, G. H. Complex coacervation: a field theoretic simulation study of polyelectrolyte complexation. *J. Chem. Phys.* **2008**, *128*, 224908.
(19) Perry, S. L.; Sing, C. E. PRISM-based theory of complex coacervation: Excluded volume versus chain correlation. *Macromolecules* **2015**, *48*, 5040−5053.
(20) Salehi, A.; Larson, R. G. A molecular thermodynamic model of complexation in mixtures of oppositely charged polyelectrolytes with explicit account of charge association/dissociation. *Macromolecules* **2016**, *49*, 9706−9719.
(21) Radhakrishna, M.; Basu, K.; Liu, Y.; Shamsi, R.; Perry, S. L.; Sing, C. E. Molecular connectivity and correlation effects on polymer coacervation. *Macromolecules* **2017**, *50*, 3030−3037.
(22) Shen, K.; Wang, Z.-G. Polyelectrolyte chain structure and solution phase behavior. *Macromolecules* **2018**, *51*, 1706−1717.
(23) Zhang, P.; Shen, K.; Alsaifi, N. M.; Wang, Z.-G. Salt partitioning in complex coacervation of symmetric polyelectrolytes. *Macromolecules* **2018**, *51*, 5586−5593.
(24) Adhikari, S.; Leaf, M. A.; Muthukumar, M. Polyelectrolyte complex coacervation by electrostatic dipolar interactions. *J. Chem. Phys.* **2018**, *149*, 163308.
(25) Chang, L.-W.; Lytle, T. K.; Radhakrishna, M.; Madinya, J. J.; Vélez, J.; Sing, C. E.; Perry, S. L. Sequence and entropy-based control of complex coacervates. *Nat. Commun.* **2017**, *8*, 1273.
(26) Rubinstein, M.; Liao, Q.; Panyukov, S. Structure of liquid coacervates formed by oppositely charged polyelectrolytes. *Macromolecules* **2018**, *51*, 9572−9588.
(27) Yu, B.; Rauscher, P. M.; Jackson, N. E.; Rumyantsev, A. M.; de Pablo, J. J. Crossover from rouse to reptation dynamics in salt-free polyelectrolyte complex coacervates. *ACS Macro Lett.* **2020**, *9*, 1318−1324.
(28) Liu, Y.; Santa Chalarca, C. F.; Carmean, R. N.; Olson, R. A.; Madinya, J.; Sumerlin, B. S.; Sing, C. E.; Emrick, T.; Perry, S. L. Effect of polymer chemistry on the linear viscoelasticity of complex coacervates. *Macromolecules* **2020**, *53*, 7851−7864.
(29) Aponte-Rivera, C.; Rubinstein, M. Dynamic coupling in unentangled liquid coacervates formed by oppositely charged polyelectrolytes. *Macromolecules* **2021**, *54*, 1783−1800.
(30) Neitzel, A. E.; Fang, Y. N.; Yu, B.; Rumyantsev, A. M.; de Pablo, J. J.; Tirrell, M. V. Polyelectrolyte complex coacervation across a broad range of charge densities. *Macromolecules* **2021**, *54*, 6878−6890.
(31) Rumyantsev, A. M.; Kramarenko, E. Y.; Borisov, O. V. Microphase separation in complex coacervate due to incompatibility between polyanion and polycation. *Macromolecules* **2018**, *51*, 6587−6601.
(32) Rumyantsev, A. M.; Gavrilov, A. A.; Kramarenko, E. Y. Electrostatically stabilized microphase separation in blends of oppositely charged polyelectrolytes. *Macromolecules* **2019**, *52*, 7167−7174.
(33) Sing, C. E. Micro- to macro-phase separation transition in sequence-defined coacervates. *J. Chem. Phys.* **2020**, *152*, 024902.
(34) Yu, B.; Rumyantsev, A. M.; Jackson, N. E.; Liang, H.; Ting, J. M.; Meng, S.; Tirrell, M. V.; de Pablo, J. J. Complex coacervation of statistical polyelectrolytes: role of monomer sequences and formation of inhomogeneous coacervates. *Mol. Syst. Des. Eng.* **2021**, *6*, 790−804.
(35) Semenov, A. N.; Khokhlov, A. R. Statistical physics of liquid-crystalline polymers. *Sov. phys. Uspekhi* **1988**, *31*, 988−1014.
(36) Chen, Z. Y. Nematic ordering in semiflexible polymer chains. *Macromolecules* **1993**, *26*, 3419−3423.
(37) Dijkstra, M.; Frenkel, D. Simulation study of the isotropic-to-nematic transitions of semiflexible polymers. *Phys. Rev. E: Stat. Phys., Plasmas, Fluids, Relat. Interdiscip. Top.* **1995**, *51*, 5891−5898.
(38) Escobedo, F. A.; de Pablo, J. J. Monte Carlo simulation of athermal mesogenic chains: Pure systems, mixtures, and constrained environments. *J. Chem. Phys.* **1997**, *106*, 9858−9868.
(39) Weber, H.; Paul, W.; Binder, K. Monte Carlo simulation of a lyotropic first-order isotropic-nematic phase transition in a lattice polymer model. *Phys. Rev. E: Stat. Phys., Plasmas, Fluids, Relat. Interdiscip. Top.* **1999**, *59*, 2168−2174.
(40) Egorov, S. A.; Milchev, A.; Virnau, P.; Binder, K. A new insight into the isotropic−nematic phase transition in lyotropic solutions of semiflexible polymers: density-functional theory tested by molecular dynamics. *Soft Matter* **2016**, *12*, 4944−4959.
(41) Milchev, A.; Nikoubashman, A.; Binder, K. The smectic phase in semiflexible polymer materials: A large scale molecular dynamics study. *Comput. Mater. Sci.* **2019**, *166*, 230−239.
(42) Rumyantsev, A. M.; Zhulina, E. B.; Borisov, O. V. Complex coacervate of weakly charged polyelectrolytes: Diagram of states. *Macromolecules* **2018**, *51*, 3788−3801.
(43) Shakya, A.; King, J. T. DNA local-flexibility-dependent assembly of phase-separated liquid droplets. *Biophys. J.* **2018**, *115*, 1840−1847.
(44) Lueckheide, M.; Vieregg, J. R.; Bologna, A. J.; Leon, L.; Tirrell, M. V. Structure-property relationships of oligonucleotide polyelectrolyte complex micelles. *Nano Lett.* **2018**, *18*, 7111−7117.
(45) Fraccia, T. P.; Smith, G. P.; Zanchetta, G.; Paraboschi, E.; Yi, Y.; Walba, D. M.; Dieci, G.; Clark, N. A.; Bellini, T. Abiotic ligation of DNA oligomers templated by their liquid crystal ordering. *Nat. Commun.* **2015**, *6*, 6424.
(46) Fraccia, T. P.; Zanchetta, G.; Rimoldi, V.; Clark, N. A.; Bellini, T. Evidence of liquid crystal-assisted abiotic ligation of nucleic acids. *Origins Life Evol. Biospheres* **2015**, *45*, 51−68.
(47) Todisco, M.; Fraccia, T. P.; Smith, G. P.; Corno, A.; Bethge, L.; Klussmann, S.; Paraboschi, E. M.; Asselta, R.; Colombo, D.; Zanchetta, G.; Clark, N. A.; Bellini, T. Nonenzymatic polymerization into long linear RNA templated by liquid crystal self-assembly. *ACS Nano* **2018**, *12*, 9750−9762.
(48) Kumar, R.; Audus, D.; Fredrickson, G. H. Phase separation in symmetric mixtures of oppositely charged rodlike polyelectrolytes. *J. Phys. Chem. B* **2010**, *114*, 9956−9976.
(49) Rumyantsev, A. M.; de Pablo, J. J. Liquid crystalline and isotropic coacervates of semiflexible polyanions and flexible polycations. *Macromolecules* **2019**, *52*, 5140−5156.
(50) Shakya, A.; Girard, M.; King, J. T.; Olvera de la Cruz, M. Role of chain flexibility in asymmetric polyelectrolyte complexation in salt solutions. *Macromolecules* **2020**, *53*, 1258−1269.
(51) Utracki, L. A. Compatibilization of polymer blends. *Can. J. Chem. Eng.* **2002**, *80*, 1008−1016.
(52) Adhikari, N. P.; Straube, E. Interfacial properties of asymmetric polymer mixtures. *Macromol. Theory Simul.* **2003**, *12*, 499−507.
(53) Qin, J.; Priftis, D.; Farina, R.; Perry, S. L.; Leon, L.; Whitmer, J.; Hoffmann, K.; Tirrell, M.; de Pablo, J. J. Interfacial tension of polyelectrolyte complex coacervate phases. *ACS Macro Lett.* **2014**, *3*, 565−568.
(54) Lytle, T. K.; Salazar, A. J.; Sing, C. E. Interfacial properties of polymeric complex coacervates from simulation and theory. *J. Chem. Phys.* **2018**, *149*, 163315.
(55) Audus, D. J.; Ali, S.; Rumyantsev, A. M.; Ma, Y.; de Pablo, J. J.; Prabhu, V. M. Molecular mass dependence of interfacial tension in complex coacervation. *Phys. Rev. Lett.* **2021**, *126*, 237801.
(56) Prabhu, V. M. Interfacial tension in polyelectrolyte systems exhibiting associative liquid−liquid phase separation. *Curr. Opin. Colloid Interface Sci.* **2021**, *53*, 101422.

https://doi.org/10.1021/acs.macromol.2c01674
Macromolecules XXXX, XXX, XXX−XXX

(57) Kremer, K.; Grest, G. S. Dynamics of entangled linear polymer melts: A molecular-dynamics simulation. *J. Chem. Phys.* **1990**, *92*, 5057−5086.
(58) Hansen, J.-P.; McDonald, I. R.*Theory of Simple Liquids*; Elsevier, 2013; pp 511−584.
(59) Everaers, R.; Sukumaran, S. K.; Grest, G. S.; Svaneborg, C.; Sivasubramanian, A.; Kremer, K. Rheology and microscopic topology of entangled polymeric liquids. *Science* **2004**, *303*, 823−826.
(60) Carrillo, J.-M. Y.; MacKintosh, F. C.; Dobrynin, A. V. Nonlinear elasticity: From single chain to networks and gels. *Macromolecules* **2013**, *46*, 3679−3692.
(61) Plimpton, S.; Hendrickson, B. Parallel molecular dynamics algorithms for simulation of molecular systems. *ACS Symp. Ser.* **1995**, *592*, 114.
(62) Brown, W. M.; Kohlmeyer, A.; Plimpton, S. J.; Tharrington, A. N. Implementing molecular dynamics on hybrid high performance computers—Particle−particle particle-mesh. *Comput. Phys. Commun.* **2012**, *183*, 449−459.
(63) Rubinstein, M.; Liao, Q.; Panyukov, S. Structure of liquid coacervates formed by oppositely charged polyelectrolytes. *Macromolecules* **2018**, *51*, 9572−9588.
(64) Ivanov, V. A.; Stukan, M. R.; Müller, M.; Paul, W.; Binder, K. Phase diagram of solutions of stiff-chain macromolecules: A Monte Carlo simulation. *J. Chem. Phys.* **2003**, *118*, 10333−10342.
(65) Stukowski, A. Visualization and analysis of atomistic simulation data with OVITO−the Open Visualization Tool. *Modell. Simul. Mater. Sci. Eng.* **2009**, *18*, 015012.
(66) Egorov, S. A.; Milchev, A.; Binder, K. Anomalous fluctuations of nematic order in solutions of semiflexible polymers. *Phys. Rev. Lett.* **2016**, *116*, 187801.
(67) Khokhlov, A. R.; Semenov, A. N. Liquid-crystalline ordering in the solution of long persistent chains. *Phys. A* **1981**, *108*, 546−556.
(68) Khokhlov, A. R.; Semenov, A. N. Liquid-crystalline ordering in the solution of partially flexible macromolecules. *Phys. A* **1982**, *112*, 605−614.
(69) Khokhlov, A. R.; Semenov, A. N. On the theory of liquid-crystalline ordering of polymer chains with limited flexibility. *J. Stat. Phys.* **1985**, *38*, 161−182.
(70) Khokhlov, A. R.; Semenov, A. N. Theory of nematic ordering in the melts of macromolecules with different flexibility mechanisms. *Macromolecules* **1986**, *19*, 373−378.
(71) Yethiraj, A.; Fynewever, H. Isotropic to nematic transition in semiflexible polymer melts. *Mol. Phys.* **1998**, *93*, 693−701.
(72) Spencer, R. K. W.; Matsen, M. W. Surface segregation in athermal polymer blends due to conformational asymmetry. *Macromolecules* **2021**, *54*, 10100−10109.
(73) Onsager, L. The effects of shape on the interaction of colloidal particles. *Ann. N.Y. Acad. Sci.* **1949**, *51*, 627−659.
(74) For simplicity, we provide the values of $\phi L/d$ and $\phi l/d$ corresponding to the spinodal positions. The positions of the binodals are known to be sufficiently close. For instance, the boundaries of the 2-phase region in Onsager model are $\phi_i L/d = 3.34$ and $\phi_a L/d = 4.49$.
(75) Parsons, J. D. Nematic ordering in a system of rods. *Phys. Rev. A Gen. Phys.* **1979**, *19*, 1225−1230.
(76) Qin, J.; de Pablo, J. J. Criticality and connectivity in macromolecular charge complexation. *Macromolecules* **2016**, *49*, 8789−8800.
(77) Chen, Z. Y. Nematic ordering in semiflexible polymer chains. *Macromolecules* **1993**, *26*, 3419−3423.
(78) Dijkstra, M.; Frenkel, D. Simulation study of the isotropic-to-nematic transitions of semiflexible polymers. *Phys. Rev. E: Stat. Phys., Plasmas, Fluids, Relat. Interdiscip. Top.* **1995**, *51*, 5891−5898.
(79) Potemkin, I. I.; Limberger, R. E.; Kudlay, A. N.; Khokhlov, A. R. Rodlike polyelectrolyte solutions: effect of the many-body Coulomb attraction of similarly charged molecules favoring weak nematic ordering at very small polymer concentration. *Phys. Rev. E: Stat., Nonlinear, Soft Matter Phys.* **2002**, *66*, 011802.
(80) Yang, D.; Venev, S. V.; Palyulin, V. V.; Potemkin, I. I. Nematic ordering of rigid rod polyelectrolytes induced by electrostatic interactions: effect of discrete charge distribution along the chain. *J. Chem. Phys.* **2011**, *134*, 074901.
(81) Odijk, T. Polyelectrolytes near the rod limit. *J. Polym. Sci., Polym. Phys. Ed.* **1977**, *15*, 477−483.
(82) Skolnick, J.; Fixman, M. Electrostatic persistence length of a wormlike polyelectrolyte. *Macromolecules* **1977**, *10*, 944−948.
(83) Barrat, J.-L.; Joanny, J.-F. Persistence length of polyelectrolyte chains. *Europhys. Lett.* **1993**, *24*, 333−338.
(84) Ha, B.-Y.; Thirumalai, D. Electrostatic persistence length of a polyelectrolyte chain. *Macromolecules* **1995**, *28*, 577−581.
(85) Dobrynin, A. V. Electrostatic persistence length of semiflexible and flexible polyelectrolytes. *Macromolecules* **2005**, *38*, 9304−9314.
(86) Rumyantsev, A. M.; Jackson, N. E.; Yu, B.; Ting, J. M.; Chen, W.; Tirrell, M. V.; de Pablo, J. J. Controlling complex coacervation via random polyelectrolyte sequences. *ACS Macro Lett.* **2019**, *8*, 1296−1302.
(87) Rumyantsev, A. M.; Johner, A.; Tirrell, M. V.; de Pablo, J. J. Unifying weak and strong charge correlations within the random phase approximation: Polyampholytes of various sequences. *Macromolecules* **2022**, *55*, 6260−6274.
(88) Brilliantov, N. V. Accurate first-principle equation of state for the one-component plasma. *Contrib. Plasma Phys.* **1998**, *38*, 489−499.
(89) Glagolev, M. K.; Vasilevskaya, V. V.; Khokhlov, A. R. Induced liquid-crystalline ordering in solutions of stiff and flexible amphiphilic macromolecules: Effect of mixture composition. *J. Chem. Phys.* **2016**, *145*, 044904.
(90) Liu, A. J.; Fredrickson, G. H. Free energy functionals for semiflexible polymer solutions and blends. *Macromolecules* **1993**, *26*, 2817−2824.
(91) Weinhold, J. D.; Kumar, S. K.; Singh, C.; Schweizer, K. S. Athermal stiffness blends: A comparison of Monte Carlo simulations and integral equation theory. *J. Chem. Phys.* **1995**, *103*, 9460−9474.
(92) Gauger, A.; Pakula, T. Phase equilibrium in mixtures of flexible and stiff polymers studied by Monte Carlo simulation. *J. Chem. Phys.* **1993**, *98*, 3548−3553.
(93) Mueller, M. Effects of structural disparities in polymer blends: A Monte-Carlo investigation. *Macromolecules* **1995**, *28*, 6556−6564.
(94) Adhikari, N. P.; Straube, E. Phase separation in mixtures of flexible and semiflexible polymers. *Polym. J.* **2011**, *43*, 751−756.
(95) Ramírez-Hernández, A.; Hur, S.-M.; Armas-Pérez, J. C.; Cruz, M. O. d. l.; de Pablo, J. J. Demixing by a nematic mean field: Coarse-grained simulations of liquid crystalline polymers. *Polymers (Basel)* **2017**, *9*, 88.
(96) Milchev, A.; Egorov, S. A.; Midya, J.; Binder, K.; Nikoubashman, A. Entropic unmixing in nematic blends of semiflexible polymers. *ACS Macro Lett.* **2020**, *9*, 1779−1784.
(97) Egorov, S. A.; Milchev, A.; Nikoubashman, A.; Binder, K. Phase separation and nematic order in lyotropic solutions: Two types of polymers with different stiffnesses in a common solvent. *J. Phys. Chem. B* **2021**, *125*, 956−969.
(98) Rumyantsev, A. M.; de Pablo, J. J. Microphase separation in polyelectrolyte blends: Weak segregation theory and relation to nuclear "pasta". *Macromolecules* **2020**, *53*, 1281−1292.
(99) Grzetic, D. J.; Delaney, K. T.; Fredrickson, G. H. Electrostatic manipulation of phase behavior in immiscible charged polymer blends. *Macromolecules* **2021**, *54*, 2604−2616.
(100) Subbotin, A. V.; Semenov, A. N. The structure of polyelectrolyte complex coacervates and multilayers. *Macromolecules* **2021**, *54*, 1314−1328.
(101) Fukuda, J. Free energy of semiflexible polymers and structure of interfaces. *Eur. Phys. J. B* **1999**, *7*, 573−583.
(102) Bolhuis, P.; Frenkel, D. Tracing the phase boundaries of hard spherocylinders. *J. Chem. Phys.* **1997**, *106*, 666−687.

https://doi.org/10.1021/acs.macromol.2c01674
Macromolecules XXXX, XXX, XXX−XXX